Published in final edited form as:

FASEB J. 2020 January ; 34(1): 237–247. doi:10.1096/fj.201902043R.

Asymmetric functions of a binuclear metal center within the transport pathway of a human zinc transporter ZIP4

Tuo Zhang[1,‡], **Dexin Sui**[1], **Chi Zhang**[1], **Logan Cole**[1], **Jian Hu**[1,2,*]

[1]Department of Biochemistry and Molecular Biology, Michigan State University, East Lansing, MI 48824

[2]Department of Chemistry, Michigan State University, East Lansing, MI 48824

Abstract

Metal clusters are exploited by numerous metalloenzymes for catalysis, but it is not common to utilize a metal cluster for substrate transport across membrane. The recent crystal structure of a prototypic Zrt-/Irt-like protein (ZIP) metal transporter from *Bordetella bronchiseptica* (BbZIP) revealed an unprecedented binuclear metal center (BMC) within the transport pathway. Here, through a combination of bioinformatics, biochemical and structural approaches, we concluded that the two physically associated metal binding sites in the BMC of human ZIP4 zinc transporter exert different functions: one conserved transition metal binding site acts as the transport site essential for activity, whereas the variable metal binding site is required for hZIP4's optimal activity presumably by serving as a secondary transport site and modulating the properties of the primary transport site. Sequential soaking experiments on BbZIP crystals clarified the process of metal release from the BMC to the bulky solvent. This work provides important insights into the transport mechanism of the ZIPs broadly involved in transition metal homeostasis and signaling, and also a paradigm on a novel function of metal cluster in metalloproteins.

Keywords

Metal cluster; Transport kinetics; Crystallography; Crystal soaking

Introduction

Many metalloenzymes exploit metal clusters for catalysis, and meanwhile, certain metal transporters, including ZnT/CDF M^{2+}/H^{+} antiporters and VIT1 Fe^{2+}/H^{+} antiporter, utilize metal clusters in the soluble domain for regulation or substrate recruitment (1,2). However, a

*Corresponding author: hujian1@msu.edu.

‡Current address: College of Food Science and Nutritional Engineering, China Agriculture University, Beijing, China 100083

Author contributions

J. H. conceived project and designed the study. T.Z., D.S, C.Z., T.L. and J.H. conducted experiments and analyzed the data. T.Z. and J.H. wrote the manuscript.

Data deposition

Atomic coordinates and structure factors have been deposited in the Protein Data Bank (PDB ID 6PGI) for the triple mutant (N178A/D208A/E240A) of BbZIP.

Conflict of interest

The authors declare that they have no conflicts of interest with the contents of this article.

metal cluster within the transport pathway of a transporter has not been often observed. One known case is sarco/endoplasmic reticulum Ca^{2+}-ATPase (SERCA), a P_{II}-type ATPase possessing a bi-calcium cluster in the middle of the transmembrane domain (3,4), but the metal cluster is not present in many other P-type ATPases transporting a variety of mono- or divalent metal ions (5–9). Besides SERCA, a recent structural study of a Zrt-/Irt- like protein (ZIP) from *Bordetella bronchiseptica* (BbZIP), which transports both Zn^{2+} and Cd^{2+} (10), revealed a bi-cadmium cluster trapped in the middle of the transport pathway (11).

The ZIP family (SLC39a) consists of thousands of transition metal transporters and universally present in all the kingdoms of life, playing central roles in transition metal homeostasis and signaling (12–15). Zinc ion appears to be the common substrate of many ZIPs, and other divalent transition metal ions (Fe^{2+}, Cd^{2+}, Mn^{2+}, Ni^{2+}, Co^{2+} and Cu^{2+}) may also be transported by some family members (12,16). In humans, a total of fourteen ZIPs have been identified and shown to be broadly involved in physiological and pathological processes (13,14,17). The human ZIPs can be further classified into four subgroups, of which the LIV-1 subfamily is the largest one and composed of nine ZIPs (ZIP4/5/6/7/8/10/12/13/14) (12). A representative LIV-1 member human ZIP4 (hZIP4) is an indispensable transporter responsible for dietary zinc uptake from small intestine, and dysfunctional ZIP4 mutations lead to a life-threatening recessive genetic disorder, Acrodermatitis Enteropathica (18,19). Sequence comparison has suggested that all the LIV-1 members possess a similar binuclear metal centre (BMC) as BbZIP and the signature motif of the LIV-1 subfamily (“HExPHExGD”) contributes to the BMC (11,20). In contrast, some other ZIPs, including ZIP1, ZIP2 and ZIP9, have a conserved lysine residue replacing a glutamate residue at the BMC of hZIP4, possibly occupying one of the metal binding sites in the BMC. A recent study on ZIP2 has shown that the lysine residue is crucial for transport activity (21). It has been hypothesized that the two associated metal binding sites (M1 and M2) in the BMC may play different roles in transport (11), but their exact functions have not yet been established.

In this work, we aim to dissect the functions of hZIP4’s BMC. We firstly conducted a bioinformatics analysis of the ZIP family members collected in the Pfam database to compare amino acid composition of the two metal binding sites. We then functionally characterized the BMC of hZIP4 through mutagenesis and zinc transport assay, and also tested the effects of mutations on substrate specificity and pH dependence. To examine the structural role of the BMC, we solved the crystal structure of a BbZIP mutant with one metal binding site (M2) being eliminated. We also conducted sequential crystal soaking experiments on BbZIP crystals to determine metal movement between the two sites and the bulky solvent. These combined efforts allowed us to conclude that the conserved transition metal binding site (M1) is the essential transport site, whereas the auxiliary site (M2) is required not only to achieve maximal zinc transport activity but also to maintain a uniform activity in a broad pH range.

Materials and Methods

Genes, plasmids and reagents

The gene encoding BbZIP from *Bordetella bronchiseptica* (NCBI reference code: WP_010926504) was synthesized (Integrated DNA Technologies) with optimized codons for expression in *Escherichia coli*. The cDNA of full length human ZIP4 (hZIP4) was obtained from Mammalian Gene Collection at Dharmacon (GenBank code: BC062625). All the mutations were made using the QuikChange mutagenesis kit (Agilent). Genes, plasmids and primers are listed in Table S1. 1-Oleoyl-rac-glycerol (Monoolein) was purchased from Sigma-Aldrich. The reagents and tools for protein crystallization were obtained from Hampton Research. Thrombin was purchased from Novagen.

Bioinformatics analysis and homology modeling

The amino acid sequences of more than 17,000 ZIPs collected in the Pfam database (PF02535) were aligned on the website (https://pfam.xfam.org/family/Zip) and analyzed in Jalview (22). After manually removing the misaligned sequences and those lacking the whole TM4 and/or TM5 (where the BMC chelating residues are located), a total of 5185 prokaryotic ZIPs, 4762 fungal/plant ZIPs and 3343 animal ZIPs were used for amino acid composition analysis. To generate the BMC structural models, homology modeling was conducted on the website of SWISS-MODEL (https://swissmodel.expasy.org/) by using the BbZIP structure (PDB ID 5TSA) as template. Metal ions were built into the model and the residue side chains were manually adjusted for reasonable geometry of metal coordination.

Cell culture, Transfection, human ZIP4 expression assay using Western blot

HEK293T cells (American Type Culture Collection) were grown in Dulbecco's modified Eagle's media (Invitrogen) supplemented with 10% (v/v) fetal bovine serum (Invitrogen) and Gibco Antibiotic-Antimycotic (Invitrogen). The plasmids used for transient transfection were prepared by Plasmid Maxi kit (Qiagen). Cells were seeded on poly-D-lysine (Corning BioCoat)-coated 24-well plate at 1×10^4 cells per well and were transfected with Lipofectamine 2000 (Invitrogen) after overnight culture. The cells were allowed to grow at 37°C for additional 24 hours before the zinc uptake assay and expression assay using Western blot.

The total expression of hZIP4-HA and its variants was detected in cell lysates by Western blot using an anti-HA antibody (Thermo Scientific Pierce). The cell surface expression level was measured by detecting the surface bound anti-HA antibodies. After washing twice with Dulbecco's phosphate-buffered saline (DPBS, Sigma-Aldrich), cells were fixed for 10 min in 4% Formaldehyde at room temperature. Cells were then washed three times with DPBS and incubated with 3 μg mL^{-1} anti-HA antibody 1 hour at room temperature. After extensive wash in DPBS to remove unbound antibodies, the cells were lysed by sonication in SDS-PAGE sample loading buffer. Cell lysates were then applied to SDS-PAGE, transferred to PVDF membranes. The anti-HA antibody in the sample was detected using HRP-conjugated goat anti-mouse IgG (Thermo Scientific Pierce, 1:2000 dilution) or goat anti-rabbit IgG (Cell Signaling Technology, 1:5000 dilution) HRP by chemiluminescence. As loading control, β-actin levels were detected using an anti-β-actin antibodys at 1:2500 dilution (Cell

Signaling Technology). The band of the heavy chain of anti-HA antibody (~50 kDa) was used for representing surface expression level of hZIP4.The surface expression levels quantitated using Image Lab (Biorad) program were used to calibrate zinc uptake activity.

Zinc uptake assay and data analysis

An improved zinc uptake assay was used to increase the dynamic range (23). In brief, HEK293T cells were washed with the washing buffer containing 10 mM HEPES pH 7.3, 142 mM NaCl, 10 mM Glucose, 5 mM KCl and then incubated with indicated concentration of $ZnCl_2$ (containing 40% $^{65}ZnCl_2$) in the Chelex-treated cell culture media at 37 °C for 20 min with occasional gentle shaking. Chelex-treated media were prepared by mixing 80 ml cell culture medium containing 10% FBS in DMEM with 10 mL Chelex® 100 resin (Biorad) for 10 min, followed by filtration of the flow through with sterilized 0.45 μm syringe filter. pH of Chelex-treated media was adjusted using HCl. Uptake was stopped by adding the same volume of stop buffer (ice-cold washing buffer containing 1mM EDTA) and cells were collect in 1.5 ml Eppendorf tubes on ice. Cells were gently washed two times by the washing buffer and lysed in 0.5% Triton X-100. Cell associated radioactivity was measured with a Packard Cobra Auto-Gamma γ-counter and the amount of zinc was calculated using a standard ^{65}Zn radioactivity curve. The zinc transport rate of the cells transfected with the empty vector was subtracted from that of the cells expressing hZIP4 or the variants. Zinc uptake rate was firstly calibrated by total protein in the sample which was measured using Bradford method (Bio Rad) and then by surface expression level (see the previous section). For comparison between the wild type protein and the variants, the calibrated transport activities were normalized by setting the activity of the wild type protein as 100%. To obtain kinetics parameters, the normalized data were fitted using the Michaelis-Menten equation.

Metal selectivity of hZIP4 was carried out with 10 μM $ZnCl_2$ (containing 40% $^{65}ZnCl_2$) plus non-radioactive $ZnCl_2$, $CdCl_2$, $CoCl_2$, $CuSO_4$, $FeSO_4$, $MnCl_2$ and $NiCl_2$ at 100 μM. 1 mM ascorbic acid was added when $FeSO_4$ was tested. Ascorbic acid did not affect zinc uptake rate of either hZIP4 expressing cells or the cells transfected with the empty vector. At least three independent experiments were conducted and three repeats were included in each experiment.

pH dependence study was conducted with 10 μM $ZnCl_2$ (containing 40% $^{65}ZnCl_2$) at pH 6.2, 6.6, 7.0, 7.4 and 7.8. Probably due to the presence of bovine serum albumin from FBS, which likely forms a protein-metal buffer in the Chelex-treated media and therefore greatly reduces free zinc ion concentration, no zinc precipitation was observed at high pH. Five independent experiments were conducted with three repeats included in each experiment. For statistics analysis of the results from five experiments, the transport activities were normalized by setting the activity at pH 6.6 as 100%. Statistical significance was tested using the Student's t-test.

Protein expression and purification

The expression of BbZIP M2 mutant was induced in the *E.coli* strain of C41 (DE3) pLysS (Lucigen) in LBE-5052 media (ref), and the cells were allowed to grow for 24 hours at room

temperature before harvest. Spheroplast were prepared (24) and suspended in a buffer containing 50 mM Tris-HCl (pH 8.0), 500 mM NaCl, 0.25 mM $CdCl_2$ and cOmplete™ protease inhibitors (Sigma-Aldrich). n-Dodecyl-β-D-Maltopyranoside (DDM, Anatrace) was added to solubilize the membrane fraction with a final concentration of 1.5% (w/v). The His_6-tagged protein was purified using HisPur™ Cobalt Resin (Thermo Scientific) in 20 mM HEPES (pH 7.3), 300mM NaCl, 5% glycerol, 0.25 mM $CdCl_2$ and 0.1% DDM. After removing imidazole using an Amicon® centrifugal filter device, the protein sample was treated with thrombin overnight at 4 °C and then loaded onto a Superdex-200 column (GE Healthcare) equilibrated with 10 mM HEPES (pH 7.3), 300 mM NaCl, 5% glycerol, 0.25 mM $CdCl_2$ and 0.05% DDM. The peak was pooled for crystallization.

Crystallization and crystals soaking

Purified BbZIP M2 mutant was concentrated to 10 mg/mL with a 30 kDa molecular weight cut-off Amicon® centrifugal filter device. The protein solution was then mixed with the molten monoolein with two coupled syringes at a ratio of 2/3 (protein/monoolein, v/v). Crystallization trials were setup using a Gryphon® crystallization robot (ARI, Inc.). 50 nl of protein-monollein mixture covered with 800 nl of well solution was sandwiched with the lipidic cubic phase (LCP) sandwich set (Hampton Research). For both wild type BbZIP and the M2 mutant, the stick-shaped crystals appeared about 2 weeks in a condition containing 33% (w/v) PEG 400, 100 mM NaCl, 100 mM $CdCl_2$, 100 mM Tris-HCl, pH 7.5 at 21 °C, and grew to full size in 4 weeks. Crystals were dehydrated with a slightly increased concentration of PEG 400, 100 mM NaCl, 100 mM $CdCl_2$ and 100 mM Tris-HCl, pH 7.5 for 24 hours before harvested with a Mitegen micromesh and flash frozen in liquid nitrogen. The crystals were soaked with metal-free soaking buffer containing 35% PEG 400, 100 mM NaCl and 100 mM Tris-HCl, pH 7.5 for 24 hours, and the zinc bound crystals were obtained by soaking the metal-free buffer soaked crystals with 35% PEG 400, 100 mM NaCl, 2 mM $ZnCl_2$ and 100 mM Tris-HCl, pH 7.5 for another 24 hours or a solution containing 100 mM $ZnCl_2$ for 2 hours.

Diffraction data collection and structure determination

X-ray diffraction data were collected at the LS-CAT (21-ID-D), GM/CA-CAT (23-ID-B and 23-ID-D) at Advanced Photon Source using a 20 μm or 10 μm beam on Eiger 9M or Pilatus3 6M detectors. LCP crystals were located and centered using the rastering approach. The datasets collected at 1.8066 Å (λ_3) were used to detect the anomalous signals of Cd^{2+}. To detect zinc specific anomalous signal in soaking experiments, two datasets were collected on the same crystal at 1.2812 Å (λ_1, which slightly shorter than the K edge of zinc at 1.2835 Å,) and 1.3225 Å (λ_2), respectively.

The diffraction datasets were indexed, integrated and scaled by HKL2000 (25). The structures, including the M2 mutant structure and those derived from the crystal soaking experiments, were solved through molecular replacement by Phaser-MR in Phenix (26) using the wild type BbZIP structure (PDB ID 5TSA) as the search template. Iterative model building and refinement were conducted in COOT (27) and Phenix.refine. For clarity, the crystallographic statistics of the datasets from crystal soaking experiments are not included in Table S4. The resolutions of crystal soaking datasets are within 2.7–3.0 Å, and the R/R_{free}

values were refined to acceptable range (R: 0.19–0.22; R_{free}: 0.22–0.29) with reasonably good geometry parameters. All the figures of protein structures were generated by PyMOL v1.3 (Schrodinger LLC).

Results

Amino acid composition of the ZIPs' BMC

We studied the ZIPs collected in the Pfam database (PF02535, including more than seventeen thousand ZIPs from all the kingdoms of life), of which approximately thirteen thousand effective sequences were analyzed with a focus on the six residues chelating the BMC in BbZIP (11). The six potential metal chelating residues are exclusively within the "P1-P2-x-x-P3" motif in the fourth and the fifth transmembrane helix. The corresponding positions are therefore referred to as TM4–1, −2, −3 and TM5–1, −2, −3, respectively. Position "x" is usually occupied by hydrophobic or small residue. The additional two residues involved in metal binding in BbZIP (M99 and E240, from TM2 and TM6, respectively) are not conserved in the proteins from higher species, and therefore excluded from this analysis. We examined the ZIPs from prokaryotes, fungi/plant and animal ZIPs separately because the features of amino acid composition in these groups are very different. As shown in Figure 1A, the residues at TM4–1 and TM5–1 only coordinate with the metal at M1, those at TM4–2 and TM5–2 only chelate the metal at M2, whereas those at TM4–3 and TM5–3 may be contributive to both metal binding sites if their side chains allow a bridging function. The structural models of a representative BMC in each group were generated through homology modeling and shown in the same orientation in Figure 1B-D. The analysis of amino acid composition reveals that the most conserved position is TM4–1 which is predominantly occupied by a histidine residue. The residue at TM5–1 is the second most conserved one and a histidine residue is highly preferred, although less than half of the prokaryotic ZIPs have a glutamine residue which participates in metal coordination at M1 in the BbZIP structure. In prokaryotes and animals, TM4–3 is primarily occupied by either an aspartate or a glutamate likely acting as a bridging residue, whereas in fungi/plants, the most prevalent is a hydrophobic residue (I/A/V/L). For another potential bridging residue at TM5–3, both prokaryotes and fungi/plants strongly prefers a glutamate, whereas the animal ZIPs prefer a histidine residue with one third of them having a hydrophobic residue at this position. Further analysis showed that, in more than 98% of the ZIPs analyzed in this work (Table S3), there is at least one carboxylate residue at either TM4–3 or TM5–3, allowing the two metal ions to be bridged by either or both of them. The residues at TM4–2 and TM5–2 are least conserved. TM4–2 is often occupied by an asparagine in prokaryotes and animals, but serine is more prevalent in fungi/plants. TM5–2 is mostly occupied by asparagine (prokaryotes), glutamine (fungi/plants) or glutamate (animal), but a lysine residue is found at this position in 10–30% ZIPs in any of the three groups. If the lysine residue adopts the same orientation as the metal chelating residues at this position, it would likely block metal binding at M2, suggesting that these ZIPs may have only one metal binding site (M1). Collectively, M1 has two highly conserved metal chelating residues at TM4–1 and TM5–1, plus one or two carboxylate residue(s) from TM4–3 and/or TM5–3, therefore representing a typical transition metal binding site containing one to three histidine residues. In contrast, although M2 likely exists in most of the ZIPs, a fraction of the ZIPs probably does not have

it because of the lysine residue at TM5–2 or at TM4–2 (only in fungi/plants). In addition, almost no histidine residue is present at M2 and therefore the metal ion at M2 would only coordinate with oxygen atoms. Taken together, sequence analysis shows that although a BMC is a common feature for most of the ZIPs, the two metal binding sites have very different amino acid composition, suggestive of different functions.

Functional characterization of hZIP4's BMC

hZIP4 is a representative animal ZIP likely possessing both M1 and M2 (11). The alanine scanning of the metal chelating residues in the BMC has shown that mutation of the bridging residue D511 at TM4–3 reduced zinc transport activity by approximately 80%, whereas single alanine substitution at other positions only moderately reduced the activity or even increased the transport rate (H540A) (11). An early study also showed that significant residual activity were detected in the mutants where each single conserved histidine residue in hZIP4 (including those in the BMC) was replaced with an alanine residue (28). In order to further clarify the role of M1 and M2 in zinc transport, we generated two variants with eliminated M1 (H507A/H536A/H540A, M1 mutant) or M2 (N508A/E537A, M2 mutant), leaving D511 unchanged so that only one metal binding site is affected with the other one being preserved. We transiently expressed the variants in HEK293T cells and conducted cell-based zinc transport assay in the Chelex-treated cell culture media. Under this condition, we recently found the activity of hZIP4 can be more accurately determined, primarily due to a largely suppressed zinc transport through the endogenous transport systems presumably by the serum proteins in the cell culture media (23). As shown in Figure 2, the M1 mutant has essentially zero zinc transport activity, even though its cell surface expression level is similar to that of the wild type protein. In contrast, the M2 mutant exhibited robust transport activity. Kinetics analysis showed no significant change in apparent K_t (corresponding to K_m for enzyme), but k_t (corresponding to k_{cat}) has been moderately reduced by approximately 30% at pH 7.4. Therefore, M2 is not essential for zinc transport, and it is only required for maximal zinc transport. Previously, an arginine was introduced at E537 and found to completely abrogate zinc transport (11). As shown in Figure 1, this position (TM5–2) can be occupied by a lysine residue in approximately 30% animal ZIPs, for instance, human ZIP1, 2 and 9. We also noticed that when TM5–2 is a lysine residue, the residue at TM4–2 is often (but not always) occupied by a serine residue, probably because the small serine can better accommodate the lysine with a long side chain. The recent study on hZIP2 has shown that this lysine is important for transport activity (21), and we were curious about the effects of permanently blocking M2 using a lysine residue on hZIP4 function. We then generated a double mutant N508S/E537K (K mutant) to mimic a ZIP with a lysine-occupied M2. Zinc transport assay showed an 80% decrease on k_t but no change on K_t. The greater k_t decrease of the K mutant than that of the M2 mutant may suggest an inhibitory effect of a positive charge at M2 on hZIP4 function, or a greater structural perturbation in the K mutant. Nevertheless, the residual activity of the K mutant again indicated that transport can be carried out even M2 is blocked by a lysine, consistent with the notion that M2 in hZIP4 is not essential for zinc transport.

It has been reported that the second metal in BMC model compounds may affect metal binding and specificity at the first site (29). We then hypothesized that M2 of hZIP4 may

play a role in modulating transport properties through its physical interaction with the transport site (M1). We firstly tested the effects of M2 elimination on substrate specificity. As shown in Figure 3A, the M2 mutant exhibited similar activity as the wild type hZIP4 in the presence of several tested divalent transition metal ions (Cd^{2+}, Co^{2+}, Cu^{2+}, Fe^{2+}, Mn^{2+} and Ni^{2+}). We then examined hZIP4's pH dependence by conducting the zinc transport assay in a range of pH from 6.2 to 7.8 (Figure 3B), which covers the physiological pH range ZIP4 may face in small intestine (18,19,30,31). Our data showed that the transport activity of the wild type hZIP4 was not sensitive to pH change. In contrast, the M2 mutant exhibited a clear pH dependence with the optimal pH at 6.6. The activity at pH 7.8 is ~30% lower than that at pH 6.6 ($P<0.01$).

Crystal structure of a BbZIP variant with eliminated M2

hZIP4 and BbZIP share 18% identical and additional 36% similar residues in the transmembrane domain, and the similarity is higher among the residues along and in the proximity of the proposed transport pathway (11). So we believe the two proteins should share fundamental structural features, particularly at the BMC. To examine whether M2 plays any structural role, we mutated the metal chelating residues at M2 in BbZIP and generated a triple mutant (N178A/D208A/E240A). The third residue (E240) is from the sixth transmembrane helix, conserved in more than half of the prokaryotic ZIPs but not present in the ZIPs from higher species. The triple mutant has a reasonably good behavior in detergent micelles and we were able to crystallize it under the same condition as the wild type protein, albeit at a lower resolution (3.5 Å). The structure was solved using molecular replacement (Table S4) and the overall structure is highly superimposable with that of the wild type protein (RMSD of C_α = 0.30 Å). As expected, no metal at M2 was observed, whereas M1 was still occupied by a Cd^{2+} (Figure 4). A close-up view showed that, except for small shift/rotation of a few amino acid side chains, neither metal position nor metal coordination sphere at M1 was significantly affected by the mutations or the absence of metal at M2. Therefore, it seems that M2 does not play a significant role in maintaining the inward-facing conformation or metal chelation at M1.

Crystal soaking experiments to determine metal movements at the BMC

In the inward-facing conformation of BbZIP, the Cd^{2+}-loaded BMC is exposed to the bulky solvent, providing us an opportunity to study the process of metal release from the BMC using crystal soaking experiments. In our previous report, it was shown that Cd^{2+} at M1 was readily replaced by externally added Zn^{2+}, whereas Cd^{2+} at M2 could not (11). This result may suggest that metal at M2 is not involved in transport. To further examine metal release from BMC, we conducted systematic crystal soaking experiments. For better comparison, all the crystallographic datasets analyzed in this work were collected on the crystals produced from the same batch of protein.

We firstly treated the Cd^{2+}-loaded crystals with EDTA, and found that although EDTA soaking did not change morphology, the crystals did not diffract at all, indicating that metal ions are required for lattice integrity. In the second trial, we soaked the crystals with the crystallization buffer containing no transition metal ions (metal-free buffer). After 24 hours, the buffer-soaked crystal still diffracted well with a similar resolution as the untreated

crystals. The structure was then solved via molecular replacement, showing no significant conformational change. Although the metal at M1 was not affected, the cadmium anomalous signal at M2 (collected at λ_3=1.8066 Å) was much lower when compared with that seen in the untreated crystals (Figure 5). For comparison among different crystals, the anomalous signals have been calibrated by using the electron density of the sulfur atoms from a set of methionine residues in the proximity of the BMC (Table S5). Concomitantly, the cadmium signal near an extracellular loop (^{119}VGPGP^{123}) between two neighboring proteins was totally gone, consistent with the notion that it is a non-specific metal binding site (Figure 4). The significantly reduced signal at M2 and the nearly unchanged signal at M1 strongly suggests that M2 has a lower affinity towards Cd^{2+} than M1 and metal at M2 can be released. We then conducted soaking experiments on the metal-free buffer-treated crystals with the crystallization buffer containing either 2 mM or 100 mM Zn^{2+}. It turned out that no zinc anomalous signal was observed at M2 in either case, whereas Cd^{2+} at M1 has been replaced by either 2 mM or 100 mM Zn^{2+} as indicated by the strong anomalous signal collected at a wavelength slightly shorter than the K-edge of zinc (λ_1=1.2812 Å) and the largely reduced signal at a wavelength longer than the K-edge (λ_2=1.3225 Å). Interestingly and unexpectedly, we found that the cadmium anomalous signal at M2 increased significantly after zinc soaking (Figure 5). Since there was essentially no Cd^{2+} in either the metal-free buffer or zinc-containing buffer, the increased cadmium signal at M2 must come from Cd^{2+} previously occupying M1, which means that some Cd^{2+} at M1 moved to M2 upon Zn^{2+} binding at M1. This result also leads to an important implication that M2 does not have an exit to release the bound metal directly to the bulky solvent, otherwise the cadmium signal would be the same or less than that seen in the metal-free buffer-treated crystals.

In sum, crystal soaking experiments indicate that: (1) Metal at M2 can be released, which means that M2 can be potentially used as an additional transport site. The possibility that metal at M2 is a staying cofactor catalyzing transport can thus be excluded; and (2) Metal at M2 needs to pass through M1 to get released, as M2 has no direct exit to the bulky solvent. A cartoon illustrating metal movements among M1, M2 and the bulky solvent in the crystal soaking experiments is shown in Figure S2.

Discussion

The ubiquitous ZIPs are crucial players in transition metal homeostasis and signaling. The crystal structure of BbZIP has revealed a unique fold and a BMC in the transport pathway, but little is known concerning the exact functions of the two physically coupled metal binding sites. In this work, we focused our research on hZIP4 and addressed this issue through a combination of bioinformatics, structural and functional approaches. Our data support a model where the two metal binding sites exert different functions in transport.

A line of evidences support M1 as the essential transport site. Firstly, sequence analysis showed that, compared with M2, M1 is a much more conserved metal binding site (Figure 1). M1 consists of at least three (very often four) metal chelating residues at the positions of TM4–1, TM4–3, TM5–1 and TM5–3, and none of these positions is occupied by a positively charged residue in the ZIPs analyzed in this work. Out of these metal chelating

residues, at least one histidine is present, consistent with the notion that M1 is evolved for binding of transition metal ions. Secondly, elimination of M1 by a triple mutation in hZIP4 led to a completely abrogated transport activity (Figure 2). By mutating three out of four metal chelating residues at M1, metal binding capability at M1 is supposed to be completely diminished. Since the M1 mutant is normally expressed at cell surface as the wild type protein, the lack of hZIP4-mediated zinc uptake for the cells expressing the M1 mutant can be largely attributed to the loss of transport activity, indicating that M1 is essential for zinc transport. Thirdly, metal removal from both sites by soaking the Cd^{2+}-loaded crystals with EDTA made the crystal lattice collapse, whereas metal removal from M2 and non-specific binding site by soaking in the metal-free buffer did not affect lattice integrity. This result implies a key role of M1 in controlling the overall conformational state, which is consistent with M1 being the transport site. Consistently, an intact M1 in the BbZIP M2 mutant is enough to maintain the inward-facing conformation (Figure 4).

In contrast, the relative low conservation in amino acid composition and the residual activity in the M2 mutant and the K mutant indicate that M2 is not absolutely required for transport. Our data showed that mutations at M2 affected hZIP4 function in two aspects.

Firstly, M2 elimination or blockage decreased transport activity. As lack of M2 in BbZIP did not lead to significant changes in either overall structure or metal coordination at M1 (Figure 4), the reduced activity of hZIP4 should not be attributed to a structural perturbation caused by the mutations. One straightforward explanation is that M2 provides the second transport site so that M2 removal or blockage by a lysine residue would reduce transport capacity from two ions per transport cycle to only one. The fact that the K mutant lost more activity than the M2 mutant may reflect a necessity to release the metal ion at M2 during transport, as a permanently positively charged entity (lysine in this work and a more bulky arginine in our previous report (11)) at M2 was shown to have additional negative effects on transport, although the potential effect of these mutations on protein structure should not be overlooked. If M2 indeed serves as a secondary transport site, it still does not contribute to an alternative transport route because of lack of an exit to the bulky solvent in the inward-facing conformation (Figure 5 and Figure S2).

Secondly, although M2 elimination did not affect substrate specificity (Figure 3A), it did slightly but substantially alter the pH dependence profile of hZIP4 (Figure 3B). This result indicates that M2 appears to be involved in a mechanism supporting efficient zinc transport in a broad pH range, which appears to be important for hZIP4's physiological function in small intestine where the pH varies from 6.6±0.5 at proximal small intestine to 7.5±0.5 at distal small intestine (30). The study of a prokaryotic SERCA homolog has shown that the pH preference of a metal transport site can be modulated by the neighboring residues (5). Different from SERCA with a bi-calcium cluster in the transport pathway, the P_{II}-type Ca-ATPase from *Listeria monocytogenes* has an arginine residue replacing a glutamate residue in Site I, and therefore binds and transports only one calcium ion per transport cycle. Biochemical studies showed that the arginine residue is required to keep an optimal transport activity at high pH, which is crucial for the bacteria to efficiently export calcium ions at a basic condition. It was proposed that deprotonation of the arginine residue at high pH removes a positive charge close to the transport site (Site II) and allows a more efficient

calcium binding, therefore accounting for a higher transport activity under basic condition (5). In a recent study of hZIP2, it was proposed that the lysine residue at M2 forms a hydrogen bond with a metal-chelating glutamate at M1 and therefore alters the latter's pK_a, allowing metal binding at the optimal pH (21). Similarly, the residues at M2 in hZIP4 may be involved in maintaining the pK_a(s) of the metal chelating residue(s) at M1 through close interactions, accounting for the altered pH dependence profile upon M2 elimination.

In conclusion, the data shown in this work support a model where M1 is the primary transport site whereas M2 plays an auxiliary role presumably by serving as an additional transport site and modulating the properties of the primary transport site (Figure 6). The asymmetric functions of the BMC distinguish hZIP4 from SERCA where both calcium binding sites were shown to be essential for transport (32). In the BMC model compounds, the two metal binding sites reciprocally affect metal binding properties (29). If this can be applied to the ZIPs, it would be conceivable that the large amino acid variations at M2 may confer a variety of properties to the ZIPs through the interactions with the primary transport site (M1), which may be key for different ZIPs to meet their specific physiological requirements. Given the critical roles of the ZIPs in transition metal homeostasis and signaling, further biochemical and structural investigations are warranted to clarify the relationship between the two metal binding sites. Structures of alternative conformations (especially the outward-facing conformation) and detailed metal binding analysis would provide key insights into how metal substrate sequentially (or parallelly) and cooperatively (or independently) binds to the BMC, which, together with the findings shown in this work, would ultimately lead to elucidation of the unique transport mechanism of the ZIPs.

Supplementary Material

Refer to Web version on PubMed Central for supplementary material.

Acknowledgments

This work was supported by NIH GM115373 and GM129004 (to J.H.).

Abbreviations

BbZIP	ZIP from *Bordetella bronchiseptica*
BMC	binuclear metal center
DDM	n-Dodecyl-β-D-Maltopyranoside
DPBS	Dulbecco's phosphate-buffered saline
hZIP4	human ZIP4
LCP	lipidic cubic phase
SERCA	sarco/endoplasmic reticulum Ca2+-ATPase
ZIP	Zrt-/Irt-like protein

References

1. Lu M, Chai J, and Fu D (2009) Structural basis for autoregulation of the zinc transporter YiiP. Nat Struct Mol Biol 16, 1063–1067 [PubMed: 19749753]
2. Kato T, Kumazaki K, Wada M, Taniguchi R, Nakane T, Yamashita K, Hirata K, Ishitani R, Ito K, Nishizawa T, and Nureki O (2019) Crystal structure of plant vacuolar iron transporter VIT1. Nat Plants 5, 308–315 [PubMed: 30742036]
3. Toyoshima C, Nakasako M, Nomura H, and Ogawa H (2000) Crystal structure of the calcium pump of sarcoplasmic reticulum at 2.6 A resolution. Nature 405, 647–655 [PubMed: 10864315]
4. Inesi G, Kurzmack M, Coan C, and Lewis DE (1980) Cooperative calcium binding and ATPase activation in sarcoplasmic reticulum vesicles. J Biol Chem 255, 3025–3031 [PubMed: 6244305]
5. Faxen K, Andersen JL, Gourdon P, Fedosova N, Morth JP, Nissen P, and Moller JV (2011) Characterization of a Listeria monocytogenes Ca(2+) pump: a SERCA-type ATPase with only one Ca(2+)-binding site. J Biol Chem 286, 1609–1617 [PubMed: 21047776]
6. Wang K, Sitsel O, Meloni G, Autzen HE, Andersson M, Klymchuk T, Nielsen AM, Rees DC, Nissen P, and Gourdon P (2014) Structure and mechanism of Zn2+-transporting P-type ATPases. Nature 514, 518–522 [PubMed: 25132545]
7. Dutta SJ, Liu J, Stemmler AJ, and Mitra B (2007) Conservative and nonconservative mutations of the transmembrane CPC motif in ZntA: effect on metal selectivity and activity. Biochemistry 46, 3692–3703 [PubMed: 17326661]
8. Mattle D, Zhang L, Sitsel O, Pedersen LT, Moncelli MR, Tadini-Buoninsegni F, Gourdon P, Rees DC, Nissen P, and Meloni G (2015) A sulfur-based transport pathway in Cu+-ATPases. EMBO Rep 16, 728–740 [PubMed: 25956886]
9. Zielazinski EL, Cutsail GE 3rd, Hoffman BM, Stemmler TL, and Rosenzweig AC (2012) Characterization of a cobalt-specific P(1B)-ATPase. Biochemistry 51, 7891–7900 [PubMed: 22971227]
10. Lin W, Chai J, Love J, and Fu D (2010) Selective electrodiffusion of zinc ions in a Zrt-, Irt-like protein, ZIPB. J Biol Chem 285, 39013–39020
11. Zhang T, Liu J, Fellner M, Zhang C, Sui D, and Hu J (2017) Crystal structures of a ZIP zinc transporter reveal a binuclear metal center in the transport pathway. Sci Adv 3, e1700344
12. Jeong J, and Eide DJ (2013) The SLC39 family of zinc transporters. Mol Aspects Med 34, 612–619 [PubMed: 23506894]
13. Lichten LA, and Cousins RJ (2009) Mammalian zinc transporters: nutritional and physiologic regulation. Annu Rev Nutr 29, 153–176 [PubMed: 19400752]
14. Takagishi T, Hara T, and Fukada T (2017) Recent Advances in the Role of SLC39 A/ZIP Zinc Transporters In Vivo. Int J Mol Sci 18
15. Taylor KM, Hiscox S, Nicholson RI, Hogstrand C, and Kille P (2012) Protein kinase CK2 triggers cytosolic zinc signaling pathways by phosphorylation of zinc channel ZIP7. Sci Signal 5, ra11
16. Antala S, and Dempski RE (2012) The human ZIP4 transporter has two distinct binding affinities and mediates transport of multiple transition metals. Biochemistry 51, 963–973 [PubMed: 22242765]
17. Anzilotti C, Swan DJ, Boisson B, Deobagkar-Lele M, Oliveira C, Chabosseau P, Engelhardt KR, Xu X, Chen R, Alvarez L, Berlinguer-Palmini R, Bull KR, Cawthorne E, Cribbs AP, Crockford TL, Dang TS, Fearn A, Fenech EJ, de Jong SJ, Lagerholm BC, Ma CS, Sims D, van den Berg B, Xu Y, Cant AJ, Kleiner G, Leahy TR, de la Morena MT, Puck JM, Shapiro RS, van der Burg M, Chapman JR, Christianson JC, Davies B, McGrath JA, Przyborski S, Santibanez Koref M, Tangye SG, Werner A, Rutter GA, Padilla-Parra S, Casanova JL, Cornall RJ, Conley ME, and Hambleton S (2019) An essential role for the Zn(2+) transporter ZIP7 in B cell development. Nat Immunol 20, 350–361 [PubMed: 30718914]
18. Wang K, Zhou B, Kuo YM, Zemansky J, and Gitschier J (2002) A novel member of a zinc transporter family is defective in acrodermatitis enteropathica. Am J Hum Genet 71, 66–73 [PubMed: 12032886]

19. Kury S, Dreno B, Bezieau S, Giraudet S, Kharfi M, Kamoun R, and Moisan JP (2002) Identification of SLC39A4, a gene involved in acrodermatitis enteropathica. Nat Genet 31, 239–240 [PubMed: 12068297]
20. Taylor KM (2000) LIV-1 breast cancer protein belongs to new family of histidine-rich membrane proteins with potential to control intracellular Zn2+ homeostasis. IUBMB Life 49, 249–253 [PubMed: 10995024]
21. Gyimesi G, Albano G, Fuster DG, Hediger MA, and Pujol-Gimenez J (2019) Unraveling the structural elements of pH sensitivity and substrate binding in the human zinc transporter SLC39A2 (ZIP2). J Biol Chem 294, 8046–8063 [PubMed: 30914478]
22. Waterhouse AM, Procter JB, Martin DM, Clamp M, and Barton GJ (2009) Jalview Version 2--a multiple sequence alignment editor and analysis workbench. Bioinformatics 25, 1189–1191 [PubMed: 19151095]
23. Zhang T, Kuliyev E, Sui D, and Hu J (2019) The histidine-rich loop in the extracellular domain of ZIP4 binds zinc and plays a role in zinc transport. Biochem J 476, 1791–1803 [PubMed: 31164399]
24. Kaback HR, and Stadtman ER (1966) Proline uptake by an isolated cytoplasmic membrane preparation of Escherichia coli. Proc Natl Acad Sci U S A 55, 920–927 [PubMed: 5327072]
25. Otwinowski Z, and Minor W (1997) Processing of X-ray diffraction data collected in oscillation mode. Macromolecular Crystallography, Pt A 276, 307–326
26. Adams PD, Afonine PV, Bunkoczi G, Chen VB, Davis IW, Echols N, Headd JJ, Hung LW, Kapral GJ, Grosse-Kunstleve RW, McCoy AJ, Moriarty NW, Oeffner R, Read RJ, Richardson DC, Richardson JS, Terwilliger TC, and Zwart PH (2010) PHENIX: a comprehensive Python-based system for macromolecular structure solution. Acta Crystallogr D Biol Crystallogr 66, 213–221 [PubMed: 20124702]
27. Emsley P, Lohkamp B, Scott WG, and Cowtan K (2010) Features and development of Coot. Acta Crystallogr D Biol Crystallogr 66, 486–501 [PubMed: 20383002]
28. Antala S, Ovchinnikov S, Kamisetty H, Baker D, and Dempski RE (2015) Computation and Functional Studies Provide a Model for the Structure of the Zinc Transporter hZIP4. J Biol Chem 290, 17796–17805
29. Yang TY, Dudev T, and Lim C (2008) Mononuclear versus binuclear metal-binding sites: metal-binding affinity and selectivity from PDB survey and DFT/CDM calculations. J Am Chem Soc 130, 3844–3852 [PubMed: 18303888]
30. Evans DF, Pye G, Bramley R, Clark AG, Dyson TJ, and Hardcastle JD (1988) Measurement of gastrointestinal pH profiles in normal ambulant human subjects. Gut 29, 1035–1041 [PubMed: 3410329]
31. Dufner-Beattie J, Wang F, Kuo YM, Gitschier J, Eide D, and Andrews GK (2003) The acrodermatitis enteropathica gene ZIP4 encodes a tissue-specific, zinc-regulated zinc transporter in mice. J Biol Chem 278, 33474–33481
32. Clarke DM, Loo TW, Inesi G, and MacLennan DH (1989) Location of high affinity Ca2+-binding sites within the predicted transmembrane domain of the sarcoplasmic reticulum Ca2+-ATPase. Nature 339, 476–478 [PubMed: 2524669]

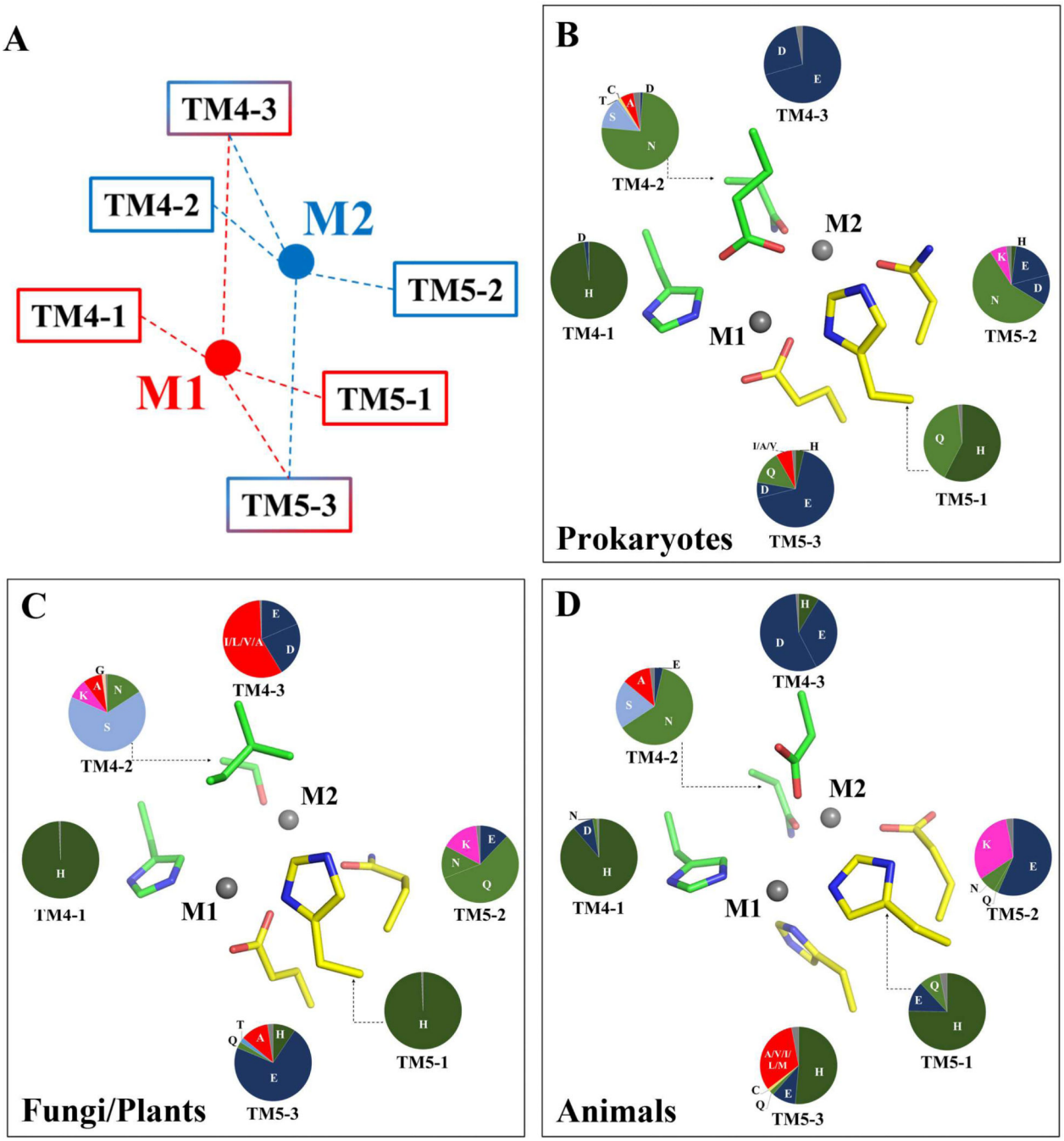

Figure 1.

Amino acid composition of the BMC. (**A**) The proposed common metal binding mode of the BMC. The dashed lines indicate the interactions between the bound metal ions and the metal chelating residues at the six positions (TM4–1,2,3 and TM5–1,2,3). (**B-D**) BMC amino acid composition of prokaryotic, fungal/plant and animal ZIPs collected in the Pfam database (PF02535). The structure model of one representative ZIP in each group was generated through homology modeling and shown stick mode (ZupT from *E.coli* for prokaryotes; IRT1 from *A.thaliana* for fungi/plants; and human ZIP4 for animals). The residues from TM4 are

in green and those from TM5 are in yellow. In the pie charts, the amino acids with a percentage equal to or greater than 1% are labeled with single letter and colored differently (H: dark green; N and Q: light green; E and D: dark blue; S and T: light blue; K: pink; A and hydrophobic residues: red; C: orange), whereas those less than 1% are combined and shown in grey.

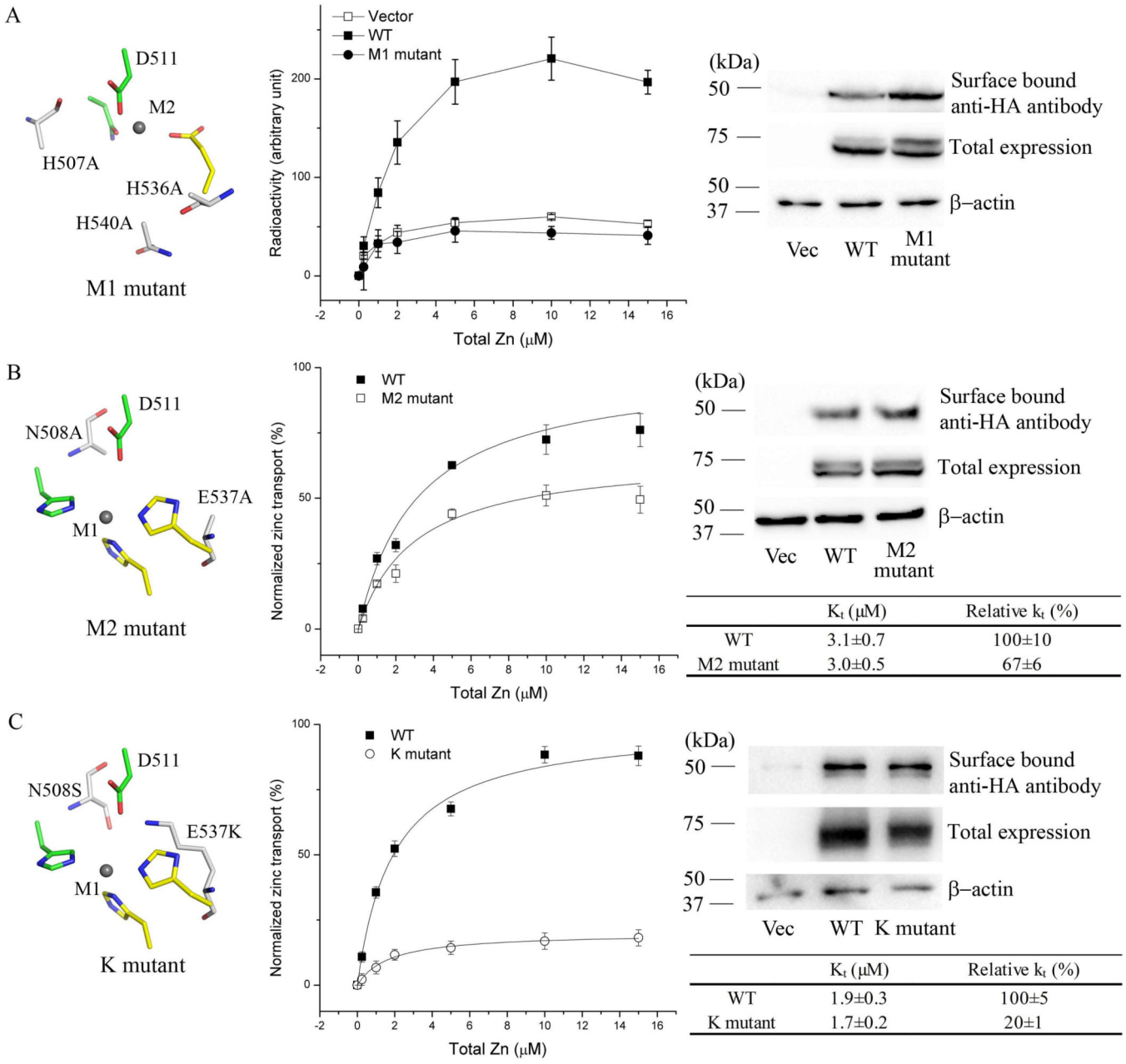

	K_t (μM)	Relative k_t (%)
WT	3.1±0.7	100±10
M2 mutant	3.0±0.5	67±6

	K_t (μM)	Relative k_t (%)
WT	1.9±0.3	100±5
K mutant	1.7±0.2	20±1

Figure 2.

Zinc uptake assay of the hZIP4 variants. (**A**) M1 mutant (H507A/H536A/H540A). (**B**) M2 mutant (N508A/E537A). (**C**) K mutant (N508S/E537K). The structural models of the variants are shown in the left column. The carbon atoms of the mutated residues are colored in white. Zinc transport assay was conducted on HEK293T cells expressing hZIP4-HA or the variants in the Chelex-treated culture media. Zinc uptake by the cells transfected with the empty vector (open square) was shown in (A), and has been subtracted in (B) and (C). The zinc transport rates in (B) and (C) have been calibrated using the surface expression level, which was quantified by the surface bound anti-HA antibody detected in Western blot. The total expression level was detected in Western blot using anti-HA antibody. The normalized

dose-dependent data was fitted to the Michaelis-Miller equation. The error bar indicates 1±S.D. The shown data are from one of at least three independent experiments.

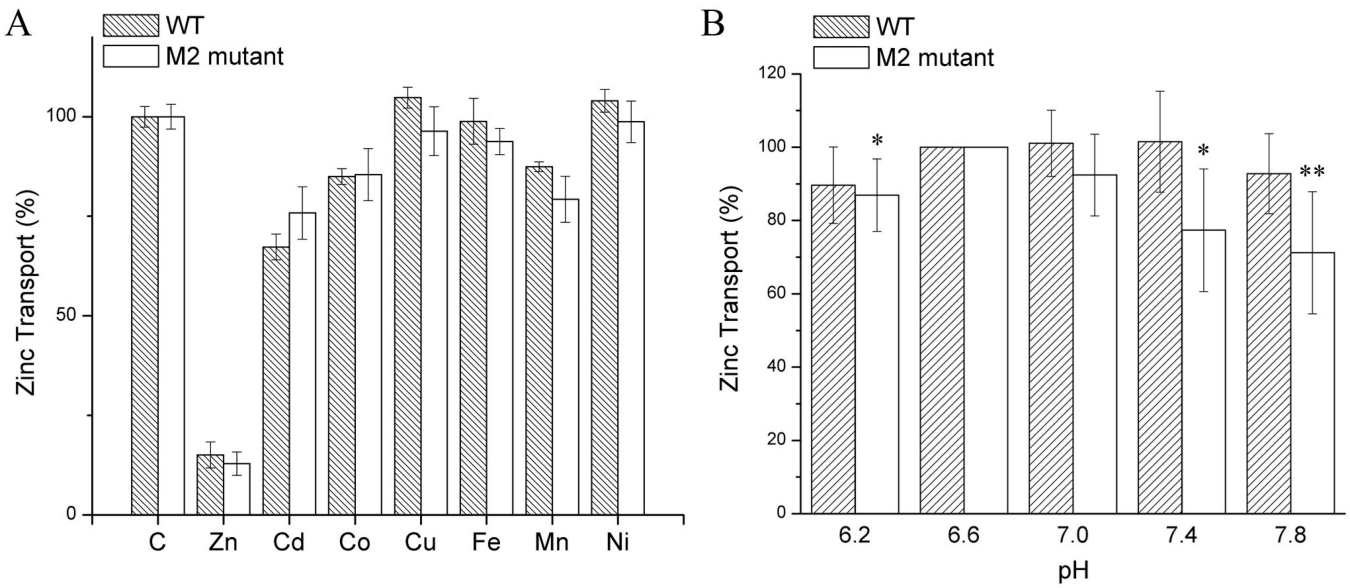

Figure 3.

The effects of M2 elimination on transport properties of hZIP4. (**A**) substrate specificity. The shown data represent one of the three independent experiments. (**B**) pH dependence. The transport activities were normalized by setting the activity at pH 6.6 as 100%, and statistics analysis were performed using the data from five independent experiments. The error bars indicate 1±S.D. Significance test between the activity at an indicated pH and that at pH 6.6 was conducted using Student's t-test. *: P<0.05, **: P<0.01.

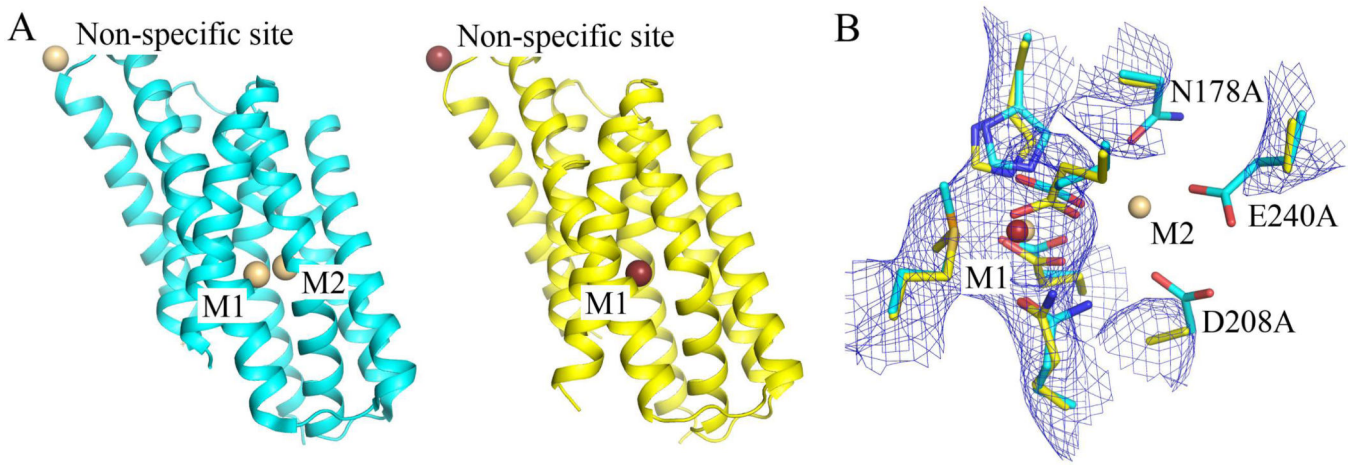

Figure 4.

Structural comparison of the triple mutant (N178A/D208A/E240A) with the wild type BbZIP. (**A**) Overall structures of the wild type BbZIP (cyan) and the mutant (yellow). The bound Cd^{2+} are depicted as light brown (in the wild type protein) and dark red balls (in the mutant), respectively. (**B**) The BMC structures. The residues are colored in the same way as in (A). The mutated residues in the variant are labeled. Note that there is no electron density at M2 in the $2F_o$-F_c map (σ=1) of the triple mutant (blue meshes).

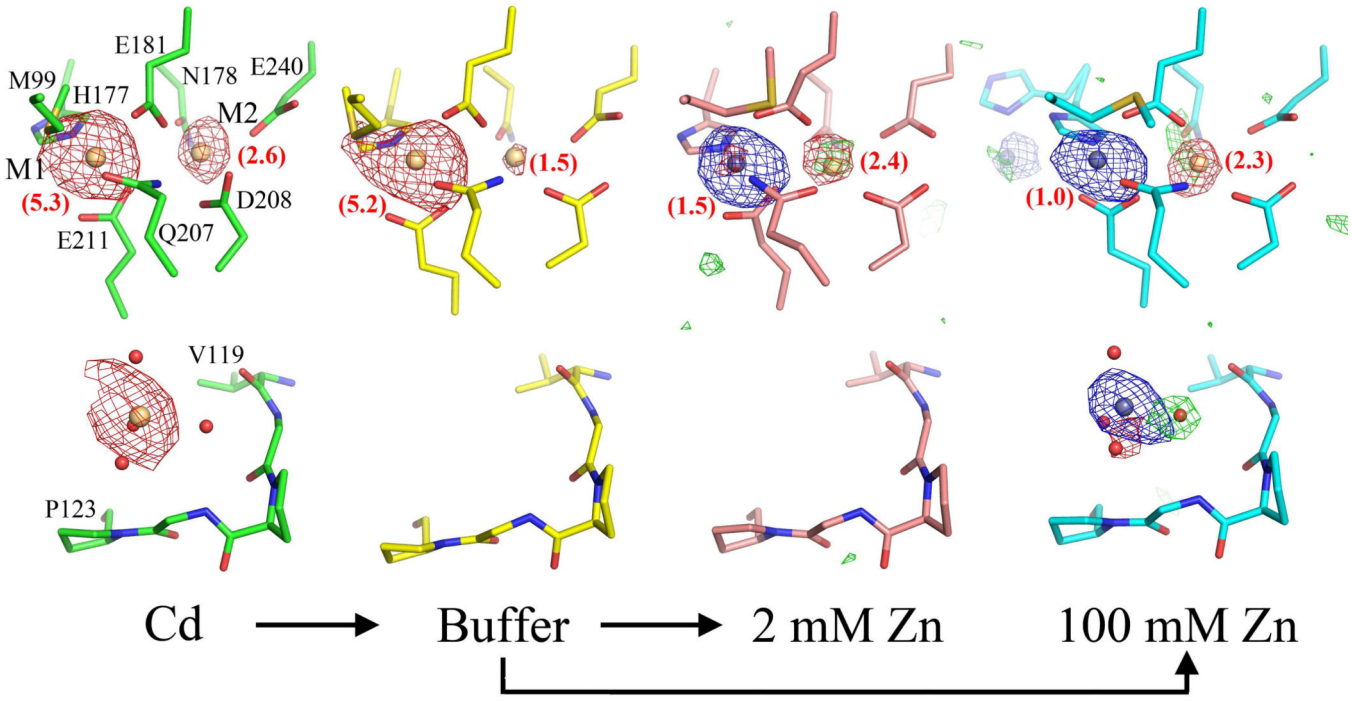

Figure 5.

Crystal soaking experiments to investigate metal movement at the BMC. The Cd^{2+}-bound crystals ("Cd", green sticks) were subjected to sequential soaking experiments indicated by arrows – they were initially soaked with the metal-free buffer ("Buffer", yellow sticks) for 24 hours at 21 °C, then soaked with the buffer containing either 2 mM Zn^{2+} (pink sticks) or 100 mM Zn^{2+} (cyan sticks) for 24 hours (for 2 mM) or 2 hours (for 100 mM). The anomalous signals at the BMC (upper panel) and a non-specific metal binding site (lower panel) are shown as blue meshes (collected at λ_1= 1.2812 Å, σ=4), green meshes (λ_2= 1.3225 Å, σ=3) and red meshes (λ_3= 1.8066 Å, σ=4). Zn generates strong anomalous signal at λ_1, which is largely reduced at λ_2, whereas Cd has larger anomalous scattering coefficient at λ_3 than that at λ_1 or λ_2 (Figure S1). Cd and Zn ions are depicted as yellow-brown and grey sphere, respectively. The small red balls represent water molecules. The residues are labeled in the "Cd" structure. The calibrated anomalous signals at λ_3 are shown in brackets. As a reference, the metal binding site near the loop (between V119 and P123) was not occupied by any metal upon soaking with metal-free buffer or 2 mM Zn^{2+}, indicative of a non-specific metal binding site.

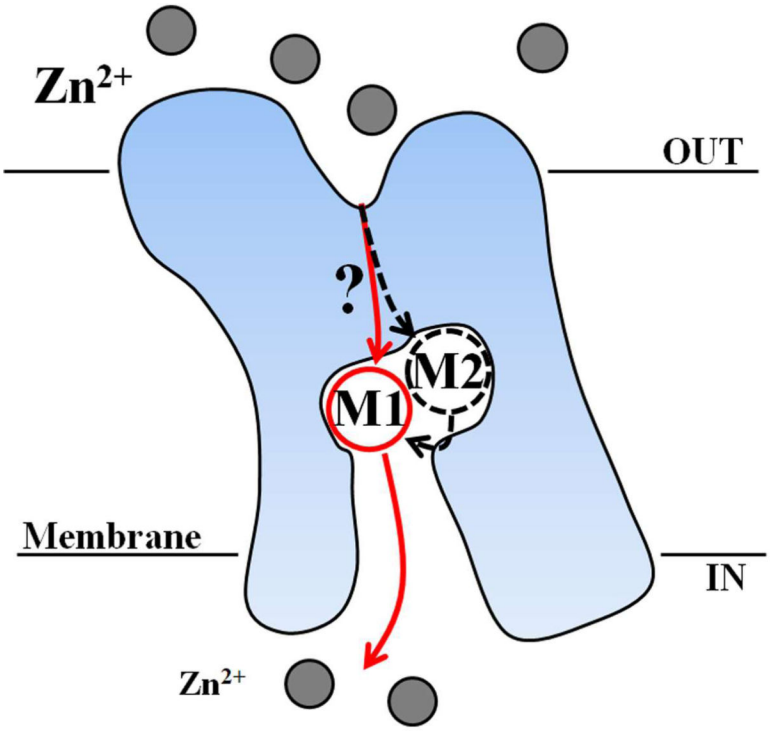

Figure 6.

Proposed functions of the BMC. M1 is the transport site absolutely required for transport activity. The transport pathway is shown with red solid arrows. M2 is an auxiliary site dispensable for transport, but needed for maximum transport activity and certain transport properties (such as pH preference). The transport pathway through M2 is shown with black dashed arrows. M2 does not have a direct exit to the cytoplasmic side, so metal at M2 needs to move to M1 and then get released. The question mark indicates the uncertainty whether metal substrate sequentially or parallelly binds to the BMC in an outward-facing conformation.